Engineering xxx (xxxx) xxx

Contents lists available at ScienceDirect

Engineering

journal homepage: www.elsevier.com/locate/eng

Research
Tunnel Engineering—Article

Adverse Geology Identification Through Mineral Anomaly Analysis During Tunneling: Methodology and Case Study

Zhenhao Xu [a,c], Tengfei Yu [a,b], Peng Lin [a,c], Shucai Li [a,b,c,*]

[a] Geotechnical and Structural Engineering Research Center, Shandong University, Jinan 250061, China
[b] School of Civil Engineering, Shandong University, Jinan 250061, China
[c] School of Qilu Transportation, Shandong University, Jinan 250002, China

ARTICLE INFO

Article history:
Received 21 June 2022
Revised 14 September 2022
Accepted 19 September 2022
Available online xxxx

Keywords:
Mineral anomaly
Adverse geology
Fault
Alteration
Anomaly threshold

ABSTRACT

Accurate and effective identification of adverse geology is crucial for safe and efficient tunnel construction. Current methods of identifying adverse geology depend on the experience of geologists and are prone to misjudgment and omissions. Here, we propose a method for adverse geology identification in tunnels based on mineral anomaly analysis. The method is based on the theory of geoanomaly, and the mineral anomalies are geological markers of the presence of adverse geology. The method uses exploration data analysis (EDA) to calculate mineral anomaly thresholds, then evaluates the mineral anomalies based on the thresholds and identifies adverse geology based on the characteristics of the mineral anomalies. We have established a dynamic expansion process for background samples to achieve the dynamic evaluation of mineral anomalies by adjusting anomaly thresholds. This method has been validated and applied in a tunnel excavated in granite. As shown herein, in the tunnel range of 142 + 800–142 + 860, the fault F_{37} was successfully identified based on an anomalous decrease in the diagenetic minerals plagioclase and hornblende, as well as an anomalous increase in the content of the alteration minerals chlorite, laumonite, and epidote. The proposed method provides a timely warning when a tunnel enters areas affected by adverse geology and identifies whether the tunnel is gradually approaching or moving away from the fault. In addition, the applicability, accuracy, and further improvement of the method are discussed. This method improves our ability to identify adverse geology, from qualitative to quantitative, and can provide reference and guidance for the identification of adverse geology in mining and underground engineering.

1. Introduction

In tunnel excavation and underground mining, adverse geological conditions such as karst, faults, and disturbance zones are often encountered [1–3]. Without timely identification and prediction measures, geohazards and engineering accidents such as collapses [4,5], water and mud inrushes [6,7], and tunnel boring machine (TBM) jamming can occur in tunnel excavation [8–11], while rockbursts [12,13], groundwater outbursts [14,15], and coal bursts can occur in underground mining [16,17]. Therefore, accurate and effective identification and prediction of adverse geological conditions are crucial for safe and efficient tunnel construction and mining [18–21]. The geological analysis method is the most commonly used method for identifying the types and properties of rock formations and forecasting the geological conditions in front of the tunnel face.

However, traditional geological analysis methods such as stereographic projection and geological cataloging mostly rely on geologists' knowledge and experience of engineering geology, hydrogeology, karst geology, and tectonic geology to qualitatively identify the types and properties of adverse geological conditions in front of the tunnel face. Consequently, such methods are often highly subjective, especially in cases of complex geological structures and deep tunnels; there is a great possibility of misjudgments and omissions. In addition, it is challenging for geologists to stay in the tunnel and work for long periods of time—especially in TBM tunnels with an excavation mileage exceeding 10 km, for which a single round-trip time can be more than 5 h. Sometimes, when encountering train deployment and water accumulation in the

* Corresponding author.
E-mail address: lishucai@sdu.edu.cn (S. Li).

https://doi.org/10.1016/j.eng.2022.09.013

roadway, a tunnel survey can take even longer, hindering the timely identification of adverse geological conditions. To address this issue, we propose a rapid identification method based on a quantitative analysis of the adverse geology of tunnels. This method transforms the traditional identification method based on geologists' experience into a less manual data analysis method and improves the effectiveness, timeliness, and accuracy of geological analysis in identifying adverse geological conditions.

Influenced by tectonic stresses and driven by geochemical effects, authigenic minerals form in adverse geological areas such as faults, alteration zones, and karsts; they have a different composition from the host rock and are known as mineral anomalies. Table 1 shows the distribution of minerals in sedimentary, igneous, and metamorphic rocks, including quartz (Qz), mica, feldspar (Fsp), magnetite, and hematite [22]. In contrast, some minerals are mainly found in specific rocks, such as clay minerals in sedimentary rock and graphite and epidote (Ep) in metamorphic rock. Thus, when minerals such as clay, graphite, and talc are found in igneous rock (usually in metamorphic and sedimentary rocks), this is considered a case of mineral anomaly, which may be caused by specific geological processes.

Tectonic stress can lead to the extensive development of fault fissures, which are favorable channels for fluid migration and accumulation. Weathering and fluid leaching lead to the enrichment of clay minerals in most fault zones [23–26], and the closer to the fault core, the more clay minerals are usually enriched (Fig. 1) [27]. The formation mechanism includes the dissolution of Fsp and mica in the protoliths and the interconversion of clay minerals. When the surrounding rock in the fault zone is granite under the leaching of acid fluids, the authigenic clay minerals are kaolinite (Kln) and montmorillonite (Mnt) [28]. When the protolith or fluid in the fault zone is rich in magnesium, the authigenic clay mineral is chlorite (Chl). When the rock composition is mainly clastic mica or alkaline Fsp, the authigenic clay minerals in the fault are either illite (Ill) or Ill-smectite mixed layers [29].

The metasomatism of gas–water hydrothermal fluids on the formed rocks leads to the accumulation of silicate, carbonate, and sulfate minerals in the affected area of the alteration zone. During the migration process of gas–water hydrothermal fluid, its chemical composition and physical and chemical conditions are constantly changing in space and time, resulting in the outward transfer of hydrothermal activity from the center. Metasomatic altered minerals usually have a pronounced zoning phenomenon. The closer to the center, the simpler the mineral combination and the greater the number of high-temperature alterations, whereas the farther away from the center, the more complex the mineral combinations and the greater the number of medium–low temperature alterations. For example, in the Denghuozhai Tunnel, the closer to the intrusive contact zone of granite and tuff, the higher the degree of alteration of the surrounding rock. There are fewer rock-forming minerals such as Qz, k-feldspar (Kfs), and plagioclase (Pl) but more authigenic minerals such as Kln and Mnt [30,31]. A large-scale mud and sand gush occurred out of the Liangshan Tunnel in Fujian Province. The diabase veins and

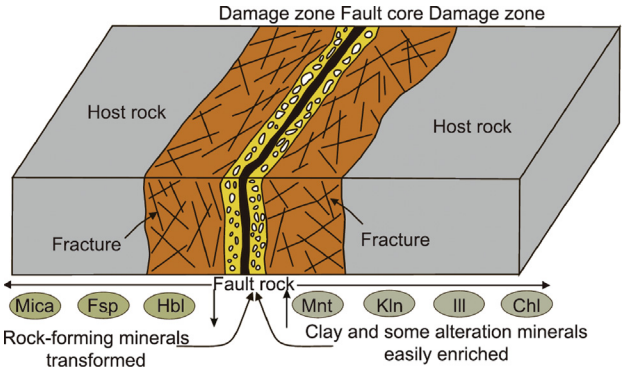

Fig. 1. A simplified diagram of mineral anomalies in a fault zone. Reproduced from Ref. [27] with permission.

the surrounding intrusive granite were altered into clay minerals, dominated by Ill and Mnt [32]. The tunnel excavation process mainly manifests anomalous mineral phenomena near the karst zones. Such phenomena are often accompanied by iron staining or clay-filled cracks near large karst caves [33].

In summary, the transformation and enrichment characteristics of minerals in adverse geological impact zones are highly correlated with the evolution of adverse geological conditions. The anomalous characteristics of minerals can be used as an identification marker for adverse geology. Based on the theory of geoanomaly, we use the concept of finding anomalies to propose an identification method for adverse geology based on the analysis of mineral anomalies. After extracting the characteristics of mineral anomalies by means of geostatistics methods, adverse geology identification is established based on mineral anomaly analysis. This method has been verified and applied in a tunnel excavated in granite. In this study, we aim to improve the identification of adverse geology by shifting it from qualitative to quantitative analysis, transform the traditional method based on geologists' experience and identification into a less manual data analysis method, and improve the effectiveness, timeliness, and accuracy of adverse geology identification in the tunnel.

2. Adverse geology identification method based on mineral anomaly analysis

2.1. Identification principle

Affected by tectonic stress and geochemical actions, mineral anomalies exist in adverse geology influence zones. A mineral anomaly is a type of geoanomaly whose changes in mineral composition and content can be used as quantitative markers to identify adverse geology. Therefore, based on the theory of geoanomalies and the establishment of the lithological sequence characteristics in a tunnel, the identification of adverse geology can be achieved by extracting and analyzing mineral anomalies using geostatistical analysis methods.

Table 1
Distribution of minerals in igneous, sedimentary, and metamorphic rocks [22].

Minerals in igneous, sedimentary, and metamorphic rocks	Minerals in igneous rock	Minerals in metamorphic rock	Minerals in sedimentary rock
Quartz (Qz), mica, rutile, feldspar (Fsp), hornblende (Hbl), pyroxene, partial garnet, olivine, magnetite, hematite, siderite, apatite, and sphene	Tridymite, leucite, nepheline, melilite, sodalite, hauyne, noselite, lamprobolite, and anorthoclase	Paragonite, epidote (Ep), serpentine, scapolite, idocrase, humite, tremolite, actinolite, periclase, aedelforsite, graphite, talc, glaucophan, chloritoid, nephrite, jadeite, andalusite, kyanite, sillimanite, corundum, cordierite, and grenatite	Opal, chalcedony, clay minerals, diaspore, saline minerals, coal, and glauconite

2.2. Extraction method for mineral anomaly characteristics

The prerequisite for mineral anomaly extraction is to determine the mineral composition and content of the rock. We used a Terra portable X-ray diffraction (XRD; Olympus, USA) instrument to test rock samples for mineral composition and content. The instrument uses Co K_α radiation and has an X-ray tube voltage of 30 kV, a current of 0.3 mA, a scanning step length of 0.05°, and a scanning range of 5°–55°. Rock samples were ground into powder with a particle size of less than 150 μm and sieved, and then 15 mg of the sample was loaded into a sample chamber. XRD patterns were obtained and then analyzed for mineral composition and content using the XPOWER software.

The main task in extracting anomaly characteristics is to determine the threshold of the mineral anomaly. When the content of a specific indicator mineral is above a certain threshold, it indicates that the mineral distribution is anomalous. Mineral anomalies can be identified through either an increase or a decrease in mineral content, corresponding to the lower or upper limits of the mineral anomalies. The application of the exploration data analysis (EDA) technique to mineral anomaly analysis is based on robust and non-parametric statistics; it does not require the mineral content data to follow a normal or log-normal distribution. Instead, this technique uses an inherent original data model to identify outliers and introduces a simple and effective graphical technique box plot (Fig. 2) [34–36]. The method is simple, practical, and suitable for analyzing mineral anomalies in tunnels.

Based on a box plot of the mineral content, the calculation method and steps to determine the mineral anomaly threshold in the rock are as follows:

(1) Sort a set of mineral content data to determine the minimum Q_{min}, median Q_{med}, and maximum Q_{max}.

(2) The median splits the mineral content data into two parts: Q_{min}–Q_{med} and Q_{med}–Q_{max}.

(3) Calculate the interquartile range, iqr = $Q_1 - Q_2$, which is also known as the inner divergence.

(4) Calculate the upper and lower inner limits. The upper inner limit is $Q_{uif} = Q_1 + 1.5iqr$, and the lower inner limit is $Q_{lif} = Q_2 - 1.5iqr$, where Q_1 is upper quartile and Q_2 is lower quartile.

(5) Calculate the mineral anomaly threshold. According to the EDA technique, the values that exceed the inner limits are outliers.

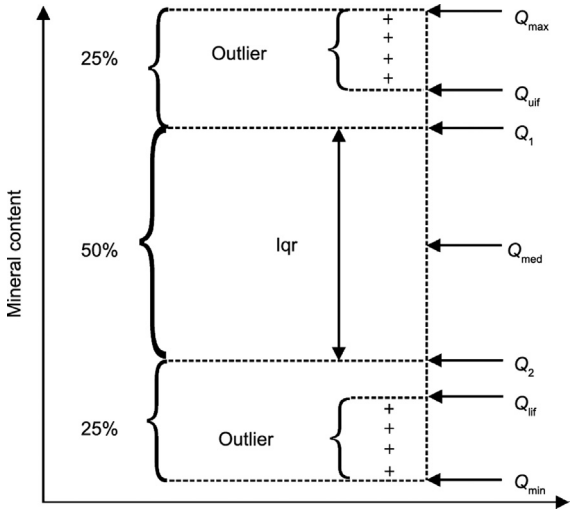

Fig. 2. EDA box plot. Q_{min}: minimum value of mineral content; Q_{med}: median value of mineral content; Q_{max}: maximum value of mineral content; Q_1: upper quartile; Q_2: lower quartile; Q_{uif}: upper inner limit; Q_{lif}: lower inner limit; Iqr: interquartile range.

Therefore, the lower limit value of a mineral anomaly is C_1 = max (Q_{lif}, 0), and the upper limit value of a mineral anomaly is C_2 = min(Q_{uif}, 1).

2.3. Identification process

Based on the principle of identification and the method for extracting the mineral anomaly threshold, a flow chart for identifying adverse geology in the tunnel is shown in Fig. 3.

The steps of the flow chart are as follows:

(1) Comprehensively analyze the geological survey data of the tunnel, including the topography and geomorphology, stratigraphic position, lithology composition, and hydrogeological and structural geological conditions, and determine possible sections of adverse geology.

(2) Follow the actual excavation mileage of the tunnel while continuously sampling and analyzing the rock and the mineral composition and content of the excavated section; establish the sequence characteristics of the mineral information of the rock.

(3) According to the established sequence characteristics of the rock in the excavated section, analyze the background value of the mineral data to form a background sample of the rock mineral data.

(4) Use EDA technology to analyze the mineral data and determine the mineral anomaly threshold of the background samples in the excavated section.

(5) Obtain and inspect the newly excavated rock mineral information. If the mineral content is within the anomalous limits, the mineral distribution is normal and is classified into the background sample to form a new background sample. Analyze the background values of the new sample data and dynamically expand the mineral background sample data.

(6) If the mineral content is outside the anomalous limits, the mineral distribution is anomalous. It is then necessary to determine whether the excavation of the lithological change zone is based on the geological prospecting data and the actual excavation exposure:

- If the tunnel is excavated into the lithological change zone, the current data sample is no longer applicable, and steps 1–5 need to be restarted.
- If the tunnel is not excavated into the lithological change zone, the mineral distribution is considered to be anomalous. Based on an analysis of the anomalous characteristics of the minerals, the identification and verification of adverse geology are carried out.

3. Engineering verification and application

3.1. Engineering geological conditions

The study area belongs to the hilly denudation area on the southern slope of the Altay Mountains. The terrain is generally lower in the north and higher in the south. The topography is not very undulating, and the bedrock is largely exposed. The study area is located in the Altai fold system and the Junggar–North Tianshan fold system. It is controlled by the Irtysh compression belt, the Junggar eugeosyncline fold belt, and the Junggar depression belt. The lithology of the stratum the tunnel passes through is mainly Carboniferous, Devonian tuff intercalated with tuff breccia, and Variscan granite. The main tunnel in the study area is 19.8 km long, of which the TBM excavation section is 17.6 km and the drilling–blasting excavation section is 2.2 km, with an average buried depth of 428 m.

There are no regional faults along the tunnel, and there are four secondary faults: F_{37}, F_{38}, F_{39}, and F_{40}. As shown in Fig. 4, the starting and ending chainage of the study area is 142 + 000–143 + 200, and the surrounding rock of the tunnel is Variscan granite. Drilling

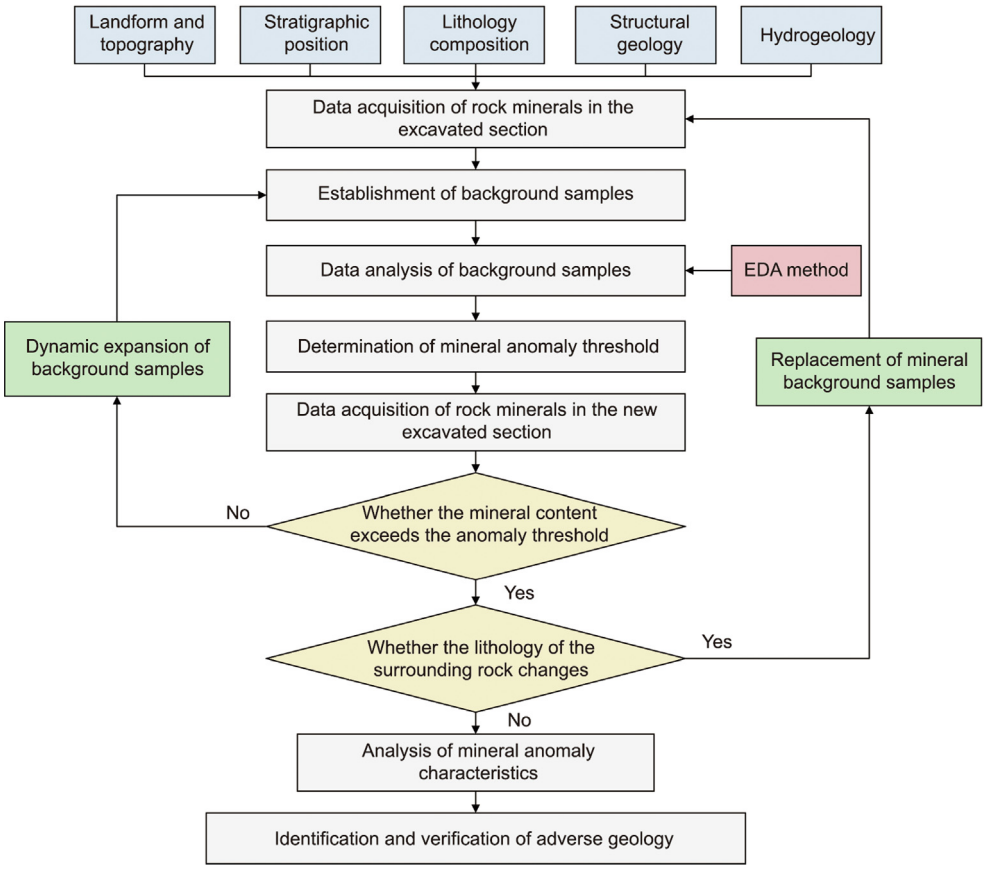

Fig. 3. Flow chart for the identification of adverse geology.

ZK63 revealed a secondary fault F_{37} with an orientation and angle of N50°W∠50°. According to the adverse geology identification process established in Section 2.3, 128 rock samples were collected from the tunnel range of 142 + 650–142 + 920. XRD diffraction spectra of some samples are shown in Fig. 5. The minerals of the surrounding rocks are mainly Qz, Pl, Kfs, Chl, hornblende (Hbl), mica, and laumontite (Lmt). (Abbreviations for all mineral species are provided in Appendix A Table S1 and all mineral content data calculated based on the height and area of the diffraction peaks are shown in Appendix A Table S2.)

3.2. Establishing initial background samples and determining anomaly thresholds

According to the identification process in Section 2.3, we first establish the mineral background samples. Fig. 6 shows a box plot of the primary mineral data of the rock in the range of 142 + 650–142 + 750. The primary mineral data of the rock can be used as the initial background sample of the mineral. The content of Pl is the highest, at about 70%–80%. The content of Qz ranks second, at 10%–20%. The content of other minerals is mostly less than 10%. The mineral data for Pl are scattered and the content varies greatly, while the other mineral data are concentrated, which is beneficial for identifying outliers. The contents of Kfs, Chl, and mica are relatively concentrated in the low range, and many rock samples do not contain these minerals, indicating that they are unstable.

The minimum value (Q_{min}), maximum value (Q_{max}), lower quartile (Q_2), and upper quartile (Q_1) of the initial mineral background sample were calculated using the data exploration analysis method. The iqr, lower limit value of the initial mineral anomaly ($C_1^{(0)}$), and upper limit value of the initial mineral anomaly ($C_2^{(0)}$) of the sample were calculated accordingly. These parameters were determined from the mineral content of 40 initial background samples, as shown in Table 2.

3.3. Mineral anomaly evaluation in the tunnel range of 142 + 750–142 + 810

The mineral anomalies in the rock samples collected in the 142 + 750–142 + 810 section were assessed using the mineral anomaly thresholds determined in Section 3.2. Data on the mineral content of the rock samples in the same section are shown in Fig. 7.

It can be seen from the comparison with the initial mineral anomaly thresholds that the contents of minerals such as Qz, Pl, and mica in the rock in 142 + 750–142 + 800 are all within the anomaly thresholds. In contrast, only one set of data—namely, Chl at 142 + 769—exceeds the anomaly threshold, while Hbl occasionally shows slight negative anomalies in 142 + 770–142 + 785. Thus, we consider there to be no apparent mineral anomalies in the range of 142 + 750–142 + 800. In the vicinity of chainage, 142 + 805, Kfs shows an apparent positive anomaly, while Hbl shows a negative anomaly. Therefore, we consider there to be no abnormal distribution of rock minerals in 142 + 750–142 + 800, which can be included in the background sample for the expansion and adjustment of sample data. The minerals of the rock in 142 + 800–142 + 810 may be in the abnormal distribution range.

3.4. Background sample expansion and anomaly threshold adjustment

According to the results of the mineral anomalies evaluation in Section 3.3, the mineral content in the range of 142 + 750–142 + 800 is normal. Combining this part of the data with the mineral

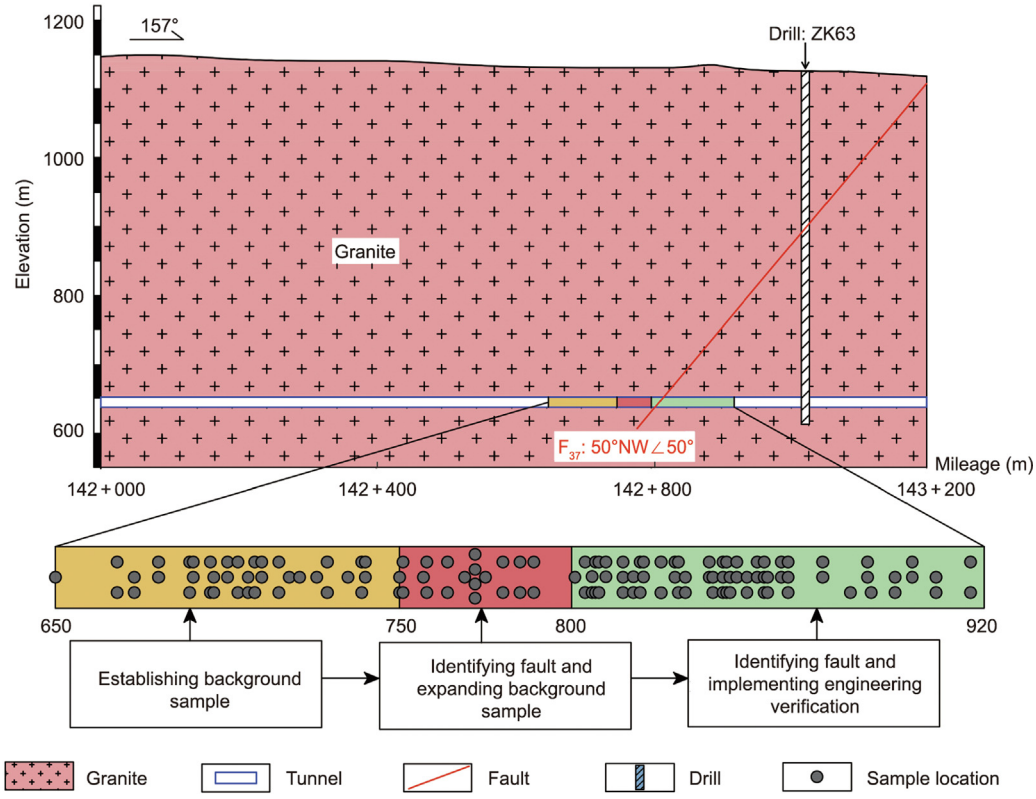

Fig. 4. Geological profile of the study area. ZK63: drill hole number.

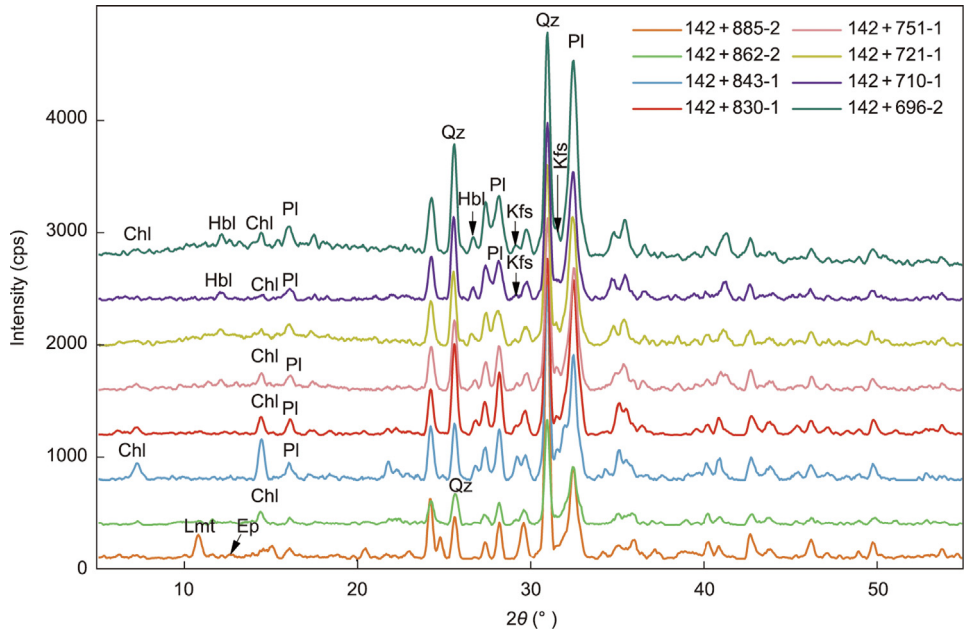

Fig. 5. XRD (Co Kα) patterns of the surrounding rock samples. cps: counts per second.

background samples, we calculate the anomaly thresholds from the mineral content of 59 background samples, as shown in Table 3. We compare the mineral anomaly limits of the initial data and the first background sample expansion, as shown in Fig. 8. There is not much difference in the anomalous upper and lower limits of Qz, Pl, muscovite (Ms), Kfs, and Chl, indicating that these minerals are fairly stably distributed in the ranges of 142 + 650–142 + 750 and 142 + 750–142 + 800. The anomalous lower limit of Hbl decreases from 0.71 to 0, while the upper limit increases from 7.10 to 7.51. This may be due to the heterogeneity of hydrothermal alteration in the fault-impacted zone, resulting in the massive decomposition of Hbl in some samples, releasing iron (Fe) and

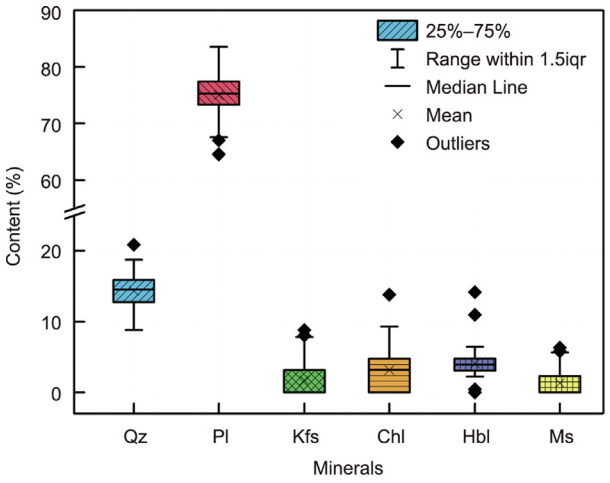

Fig. 6. Mineral content box plot of rock samples in the 142 + 650–142 + 750 section. Ms: muscovite.

calcium (Ca). In contrast, Hbl does not decompose in some samples and remains present at a high level.

3.5. Evaluation of mineral anomalies in the tunnel range of 142 + 800–142 + 920

The mineral contents of the rock samples in the tunnel range of 142 + 800–142 + 920 were assessed using the anomaly thresholds adjusted for the first time in Section 3.4. As shown in Fig. 9, according to the mineral anomaly thresholds after the first adjustment, the Qz, Kfs, and mica of the rocks in 142 + 800–142 + 830 show positive anomalies, and the Pl shows negative anomalies. Kfs and Chl in the 142 + 840–142 + 860 section show positive anomalies, while Pl shows negative ones. The range of Qz contents increases, with some above the upper limit of the anomaly and some below the lower limit of the anomaly.

Many authigenic minerals, such as Ep and laumonite, were detected in the rock samples within the mineral anomaly range mentioned above. Compared with the presence of Ep and laumonite in the 142 + 750–142 + 810 range, the continuous occurrence of Ep in 142 + 800–142 + 850 and the relatively high zeolite content in 142 + 840–142 + 860 indicated that there was a significant mineral anomaly in 142 + 800–142 + 860. Meanwhile, no Hbl was detected in the rock samples in 142 + 810. Although the anomaly threshold was not exceeded after the first adjustment, the Hbl content was significantly lower than that in the previous range, which was also evidence of mineral anomalies in this tunnel range. In 142 + 885–142 + 905, aside from Qz, Kfs, and mica, Pl showed negative anomalies. There were no abnormalities in other parts and other minerals. The rock samples in the 142 + 860–142 + 920 range contained only low Ep and Lmt, which were also detected at the chainage of 142 + 885.

3.6. Adverse geology identification and engineering verification

Following the identification process introduced in Section 2.3, we used the adverse geology identification method based on the mineral anomaly analysis, combined with knowledge of the structural geology and rock mineralogy, to gradually identify and verify the F_{37} fault.

3.6.1. Identification and verification in the tunnel range of 142 + 800–142 + 830

First, mineral anomalies start to appear at the chainage of 142 + 800. The result of the anomaly evaluation is that Kfs has a positive anomaly, while Hbl has a negative anomaly. According to the geoanomaly theory, starting from the chainage of 142 + 800, the tunnel may enter the fault F_{37} impact zone. The mineral anomalies of the rock in the tunnel range of 142 + 800–142 + 830 show positive anomalies of Qz, Kfs, and mica. At the same time, Pl is greatly reduced, while more content of Ep begins to appear. Under certain temperature and pressure conditions, mafic minerals such as Hbl will release Fe and Ca during the chloritization process, and Pl can form Ep under the metasomatism of Fe- and Ca-rich hydrothermal fluids [37]. The reaction formula may be expressed as follows:

$$2NaAlSi_3O_8\ [albite] + 2Ca^{2+} + Fe^{3+} + 3H_2O = Ca_2FeAl_2Si_3O_{12}(OH)[Ep] + 2Na^+ + 5H^+ + 3SiO_2$$

The positive anomaly of Qz may be related to the epidotization of Pl. SiO_2 in the hydrothermal fluid and SiO_2 decomposed from the original silicate minerals are pre-precipitated to form veins. The increase in Kfs and mica content may be related to feldsparization of potassium and sericitization of Pl.

Starting from the chainage of 142 + 800, the stability of the tunnel's surrounding rock gradually deteriorated, and a slight rock fall occurred at the tunnel vault (Fig. 10(a)). Significant epidotization can be observed at 142 + 815, with increased fractures in the rock at 142 + 818 and the formation of tiny veins (Fig. 10(b)).

3.6.2. Identification and verification in the tunnel range of 142 + 830–142 + 860

As the tunneling continues, the previous apparent mineral anomalies remain in the range of 142 + 830–142 + 860. Pl still shows negative anomalies, while Kfs and Chl show positive anomalies. A great deal of authigenic laumonite is detected in the surrounding rock. There is no Hbl mineral in the surrounding rock of this section, so we believe that all the Hbl in this section may have been altered into Chl, resulting in the fluid being rich in Fe and Ca. Pl can be converted to Lmt under the action of Ca-rich hydrothermal fluid [38]. The conversion reaction formula can be written as follows:

$$CaAl_2Si_2O_8\ [anorthite] + 2H_4SiO_4 = CaAl_2Si_4O_{12}{\cdot}4H_2O\ [Lmt]$$

$$2NaAlSi_3O_8\ [albite] + Ca^{2+} + 4H_2O = CaAl_2Si_4O_{12}{\cdot}4H_2O\ [Lmt] + 2Na^+ + 2SiO_2$$

Table 2
Mineral anomaly thresholds determined from 40 initial background samples.

Parameters	Qz	Pl	Kfs	Chl	Hbl	Ms
Q_{max}	18.72	83.58	8.81	13.77	14.13	6.33
Q_{min}	8.81	64.55	0	0	0	0
Q_1	15.80	77.41	2.91	4.73	4.70	2.18
Q_2	12.78	73.32	0	0	3.10	0
iqr	3.02	4.09	2.91	4.73	1.60	2.18
$C_1^{(0)}$	8.24	67.18	0	0	0.71	0
$C_2^{(0)}$	20.34	83.55	7.27	11.82	7.10	5.46

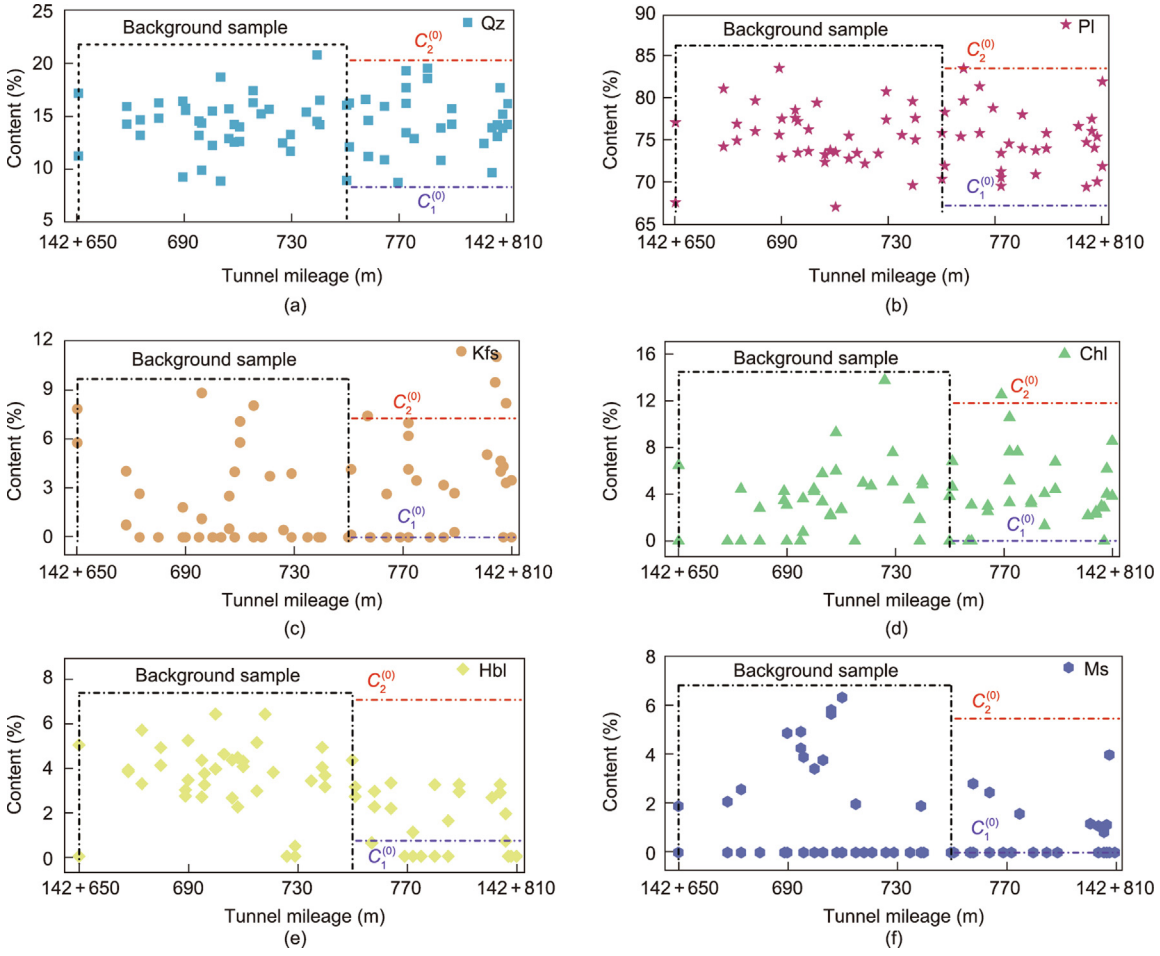

Fig. 7. Mineral contents of samples in the tunnel range of 142 + 650–142 + 810: (a) Qz, (b) Pl, (c) Kfs, (d) Chl, (e) Hbl, and (f) Ms.

Table 3
Mineral anomaly thresholds determined by 59 background samples.

Parameter	Qz	Pl	Kfs	Chl	Hbl	Ms
Q_{max}	20.84	83.58	8.81	13.77	14.13	6.33
Q_{min}	8.67	64.55	0	0	0	0
Q_1	16.12	77.53	3.58	5.00	4.32	1.88
Q_2	12.71	73.29	0	1.05	2.19	0
iqr	3.41	4.23	3.58	3.96	2.13	1.88
$C_1^{(1)}$: first adjusted lower limit value of the mineral anomaly	7.59	66.94	0	0	0	0
$C_2^{(1)}$: first adjusted upper limit value of the mineral anomaly	21.24	83.88	8.95	10.94	7.51	4.71

The tunneling revealed small altered rock veins at 142 + 843, and many cracks were formed in the surrounding rock (Fig. 11(a)). The surrounding rock of the vault was severely fractured and collapsed at 142 + 848.6, so it can be inferred that a damage zone was formed by the development of the fault F_{37} (Fig. 11(b)). A large area of granite at 142 + 855 was altered into Lmt, indicating that the gas–water hydrothermal fluid metasomatic alteration is significant. As a result, the stability of the surrounding rock is poor (Fig. 11(c) and (d)).

3.6.3. Identification and verification in the tunnel range of 142 + 860–142 + 920

At the tunnel range of 142 + 860–142 + 880, Pl and Kfs slightly exceed the anomaly thresholds, and the rock at 142 + 862 is relatively intact (Fig. 12(a)). In the range of 142 + 880–142 + 900, Pl shows negative anomalies. In contrast, Kfs and Qz show positive anomalies. A small amount of Ep and Lmt is detected at 142 + 885. Therefore, we infer that the mineral anomaly here is also affected by the development of fault F_{37}, and the broken surrounding rock is caused by hydrothermal alteration. The contents of Pl, Kfs, and Qz in the 142 + 900–142 + 920 range return to normal and do not exceed the threshold of the anomaly. After the chainage of 142 + 900, the minerals in the surrounding rock are no longer anomalous, and the surrounding rock is generally intact. The tunneling is also moving away from fault F_{37} (Fig. 12(b)).

3.7. Overall identification results

The overall identification results of fault F_{37} are shown in Fig. 13. We used the surrounding rock mineral data of 142 + 650–142 + 750 as the initial background sample and calculated the initial mineral anomaly thresholds according to the data explo-

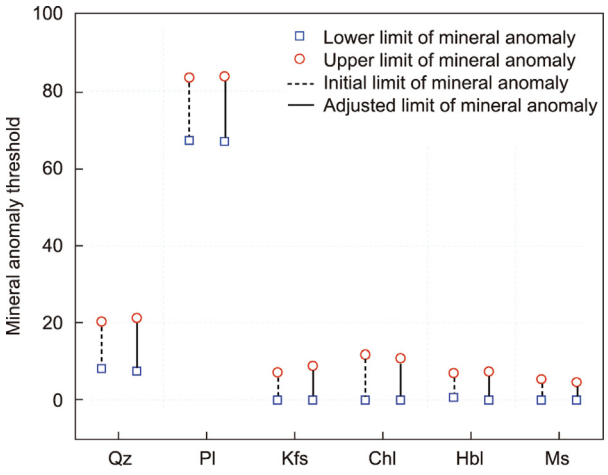

Fig. 8. Comparison of the initial and the first adjusted mineral anomaly limits.

ration and analysis technology. After preliminary mineral abnormality evaluation, we found that the mineral content of the rock in the range of 142 + 750–142 + 800 does not exceed the anomaly threshold. We incorporated this part of the mineral data into the background sample and adjusted the anomaly threshold. The evaluation of mineral anomalies continued with the excavation of the tunnel. The results showed that there are apparent anomalies in Pl, Kfs, Chl, Ep, and Lmt minerals in the range of 142 + 800–142 + 860. A large amount of Hbl has been transformed into Chl and released Fe and Ca, which then caused Fsp to be altered to Ep and laumonite. The content of altered minerals in the rock at some chainages exceeds 60%. This section of the tunnel is close to the fault core, in which the surrounding rock is fractured, cracks have developed, the vault has collapsed severely, and the degree of mineral anomalies is high. In the range of 142 + 860–142 + 900, the degree of mineral anomalies lessens. After the chainage of 142 + 900, the mineral content of Pl, Chl, Ep, and Lmt return to normal, and the surrounding rock in the tunnel gradually becomes intact.

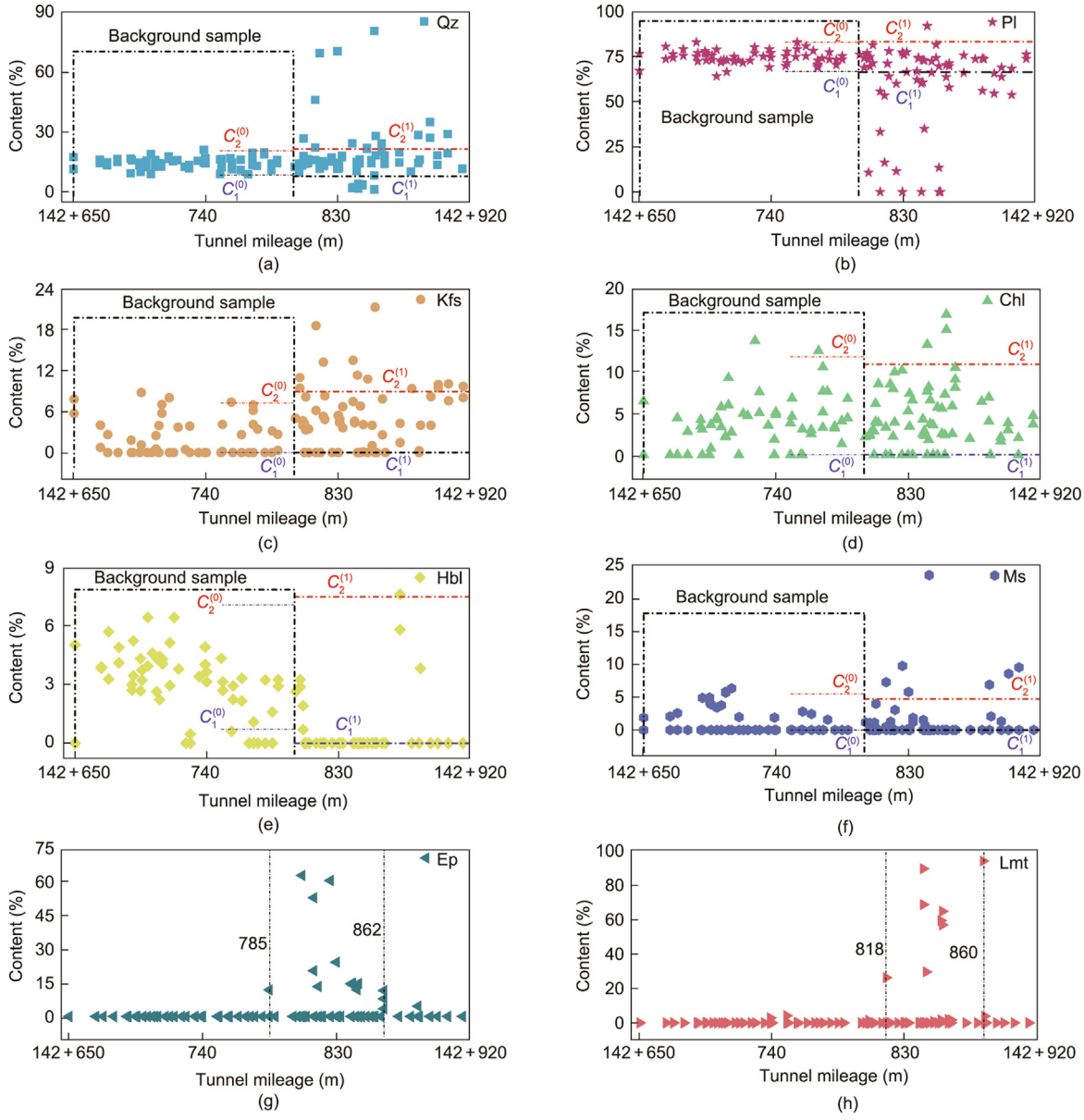

Fig. 9. Mineral contents of rock samples in the 142 + 650–142 + 920 range: (a) Qz; (b) Pl; (c) Kfs; (d) Chl; (e) Hbl; (f) Ms; (g) Ep; and (h) Lmt.

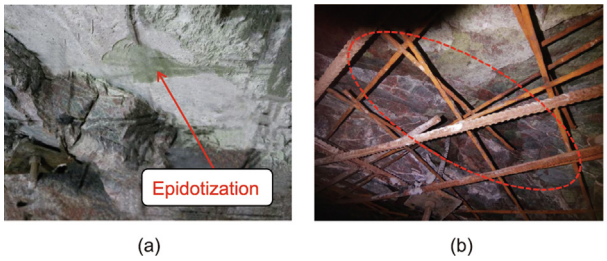

Fig. 10. Macro characteristics of the rock in the range of 142 + 810–142 + 830. (a) Epidotization granite at the chainage of 142 + 815; (b) small veins developed at the chainage of 142 + 818.

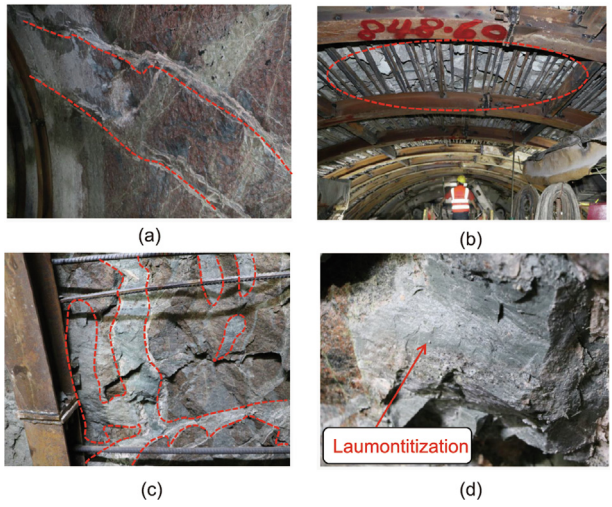

Fig. 11. Macro characteristics of the rock in the rang of 142 + 830–142 + 860 in the tunnel. (a) Small altered rock veins at 142 + 843, (b) the tunnel vault collapsed at 142 + 848.6, (c) altered veins at 142 + 855, (d) laumontitization of granite at 142 + 855.

Fig. 12. Macro characteristics of the rock in the 142 + 860–142 + 920 range of the tunnel. (a) Surrounding rock at 142 + 862 and (b) surrounding rock at 142 + 910.

The above practical engineering verification shows that the mineral anomalies of the surrounding rock in the tunnel have a specific correlation with the location of fault F_{37}. The greater the degree of mineral anomaly, the more severe the substantial alteration of the surrounding rock (broken, cracks developed, and poor stability), and the closer the tunnel is to the fault core.

4. Discussion

4.1. Applicability and accuracy of the identification method

The adverse geology identification method based on mineral anomaly analysis established in this paper can effectively determine whether a tunnel is entering areas affected by any adverse geology. The proposed method can also identify and predict whether the tunnel is gradually approaching or moving away from the adverse geology. The principle of the identification method is to continuously obtain the mineral composition and content of the rock in the tunnel and then use a statistical method to determine whether it is abnormal. Therefore, regardless of whether the tunnel is excavated using the drilling-blasting method or the TBM method, it is only necessary to continuously collect rock samples of the tunnel, obtain the sequence characteristics of the mineral composition and content, and perform an anomaly evaluation. It is then possible to quickly identify adverse geology. So far, this method has had no impact on the tunnel construction. The approach does not need to be implemented by geologists or engineers with special expertise and extensive experience; only the ability to analyze mineral tests and anomalies is needed.

Different scales of adverse geology cause different degrees of modification to surrounding geological bodies. For example, large-scale fault zones and altered zones can significantly change the geochemical properties and mineral composition of the surrounding geological bodies, resulting in an extensive range of geological anomalies. Geological anomalies caused by large-scale adverse geology can therefore be easily identified. Anomalous features are minimal when the influence range of adverse geological bodies is small, such as when the width of the entire alteration zone is less than 1 m (Fig. 14(a)). In such cases, it is challenging to identify noticeable mineral anomalies. The adverse geology identification method based on mineral anomaly analysis proposed in this paper depends on judging the mineral anomalies in the surrounding rock. Therefore, the scale of the adverse geology will significantly affect the accuracy of the method. The larger the scale of the adverse geology, the more pronounced the mineral anomaly reflected in the surrounding rock, and the higher the identification accuracy of this method. Conversely, when the scale of the adverse geology is small and the geological anomaly is not apparent, the accuracy of the identification method will be reduced or the method may even be ineffective. However, minor adverse geology only has a slight impact on tunneling; TBMs can generally pass through safely and quickly with compliant excavation and support methods.

According to the theory of geoanomaly, the evolution of adverse geology must be based on the existence of mineral anomalies. Still, mineral anomalies do not necessarily mean the presence of adverse geological bodies. For example, mineral anomalies can also occur when the collected mineral data come from veins or mineral aggregates (Fig. 14(b)). In such cases, the changes are due to crystallization differentiation in the rock rather than to adverse geological processes, and the surrounding rock only shows differences in mineral types and contents, without showing the transformation process of diagenetic minerals to clay or alteration minerals. Therefore, the pattern of mineral anomalies can be used to determine whether the anomalies are caused by adverse geological processes. Thus, the method is suitable for tunnels excavated by drilling–blasting or TBM, and is particularly suited for identifying large-scale adverse geology with mineral anomalies, such as faults, alteration zones, and karst. In contrast, this method is not applicable for identifying adverse geology without mineral anomalies, such as rock bursts caused by high ground stress.

We used geostatistical methods to analyze and extract mineral anomaly information in this study. Therefore, the number of rock samples and their representativeness are prerequisites for the anomaly analysis and accurate identification of adverse geology. In reality, it is difficult to obtain complete data for the whole geological body, and geological data are mainly obtained from samples collected along or on the surface of the geological body according to specific sampling rules [39]. In this study, we continuously collected rock samples following the mileage variation of the tunnel.

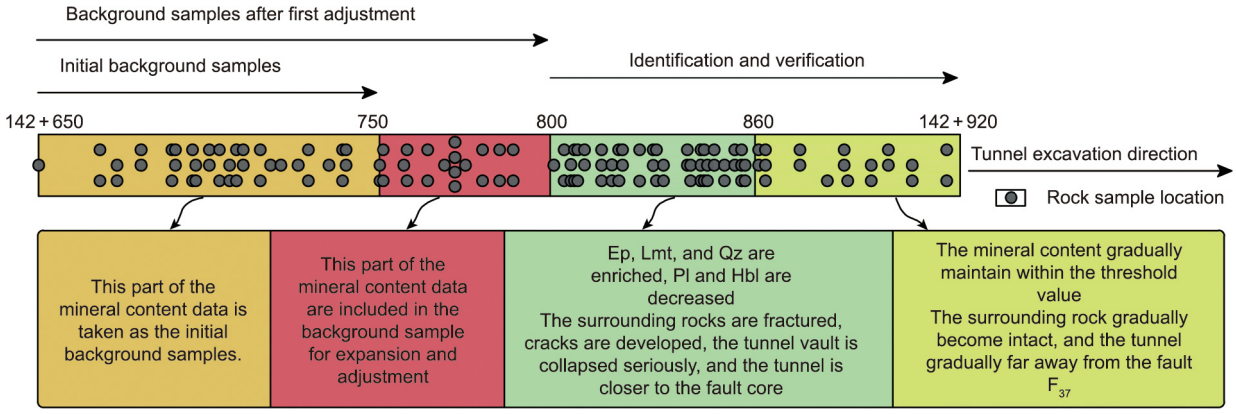

Fig. 13. Overall identification results.

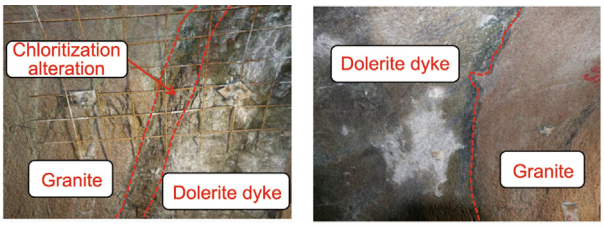

Fig. 14. Mineral anomalies are difficult to identify and can be misidentified. (a) Chloritization alteration occurred in the contact zone between granite and dolerite dyke and (b) dolerite dyke interspersed in granite.

Nevertheless, whether it is a normal surrounding rock zone or an adverse geology influence zone, as many rock samples as possible should be taken at the engineering site. The more sample data are available that can better reflect the mineral changes of the adverse geological body and the surrounding area, the better the adverse geology identification will be. In addition, the representativeness of samples within the adverse geology influence zone should be considered, because rock samples with different colors and structures may reflect different mineral anomaly patterns. Missing representative samples may not reflect all mineral anomaly information [40], leading to inaccurate results of adverse geological identification.

4.2. Further improvement of the identification method

The proposed identification method is based on the theoretical basis that mineral anomalies exist in adverse geology-affected areas. The pattern of mineral anomalies in areas affected by adverse geology is often complex and variable. Geological processes that affect mineral anomalies include surficial weathering, hydrothermal alteration, and fluid leaching. Most scholars believe that adverse geology influence zones are often rich in clay minerals such as Kln, Mnt, and Ill, or in alteration minerals such as Chl, serpentine, and talc [23–26]. Usually, these indicator minerals do not appear alone but in multiple combinations, which further increases the difficulty of using mineral anomalies to identify the type and nature of adverse geology. Factors that control the anomalous mineral characteristics of adverse geology-affected zones are the rock lithology, fluid composition, stress, temperature, and pressure conditions. In future studies, we plan to combine numerous engineering cases to analyze the regularity of mineral anomalies in adverse geology influence zones, provide prior knowledge for the adverse geology identification method based on the anomaly analysis of mineral data, and further improve the accuracy and effectiveness of this identification method.

We used portable XRD for mineral composition and content analysis in this study. However, hyperspectral technology, which has the advantage of rapid and nondestructive analysis of rock minerals, has been widely used in borehole core cataloging and mineral mapping and could be a better alternative to XRD [41–44]. Thus, a future research direction is how to improve the accuracy of hyperspectral techniques for mineral testing under the tunnel conditions of humidity, insufficient light, and dust interference. In addition, the expansion of background samples in this study relied on manual adjustment, which cannot yet realize the real-time dynamic expansion of background samples and the real-time analysis of thresholds in the process of mineral anomaly analysis. Therefore, future research will focus on optimizing the dynamic expansion method of background samples, developing matching data analysis and processing software, and realizing the real-time dynamic expansion and analysis of background samples and thresholds. Furthermore, the future development of automatic testing devices for minerals in tunnels can be expected to occur through a combination of artificial intelligence and big data analysis technology, which will eventually decrease the need for manual analysis and realize the unmanned intelligent identification of adverse geology based on mineral anomaly analysis.

5. Conclusions

In this work, we proposed an adverse geology identification method based on the analysis of mineral anomalies. This method is grounded on the theory of geoanomaly, with mineral anomalies as precursor features for the existence of adverse geology and mineral types and contents as indicators for the identification of adverse geology. The main conclusions are as follows:

(1) The proposed method uses EDA to calculate mineral anomaly thresholds; it then evaluates the mineral anomalies and identifies adverse geology such as faults and alteration zones based on the characteristics of the mineral anomalies. We established a dynamic expansion process for background samples and implemented the dynamic evaluation of mineral anomalies by adjusting anomaly thresholds.

(2) The method has been validated and applied in a tunnel constructed in granite. The fault F_{37} was successfully identified based on the anomalous decrease in the diagenetic minerals Pl and Hbl, as well as the anomalous increase in the content of the alteration minerals Chl, laumonite, and Ep. The method provides a timely warning when a tunnel enters an area affected by adverse geology and can identify whether the tunnel is gradually approaching or moving away from the fault.

(3) The method is suitable for tunnels excavated by drilling–blasting or TBM and is particularly suited for identifying large-scale adverse geology, such as faults and alteration zones.

(4) This method transforms the identification method of adverse geology from qualitative to quantitative.

Acknowledgments

We would like to acknowledge financial support from the National Natural Science Foundation of China (52022053 and 52009073) and the Natural Science Foundation of Shandong Province (ZR201910270116).

Compliance with ethical guidelines

Zhenhao Xu, Tengfei Yu, Peng Lin, and Shucai Li declare that they have no conflict of interest or financial conflicts to disclose.

Appendix A. Supplementary data

Supplementary data to this article can be found online at https://doi.org/10.1016/j.eng.2022.09.013.

References

[1] Deng MJ. Challenges and thoughts on risk management and control for the group construction of a super-long tunnel by TBM. Engineering 2018;4(1):112–22.
[2] Zhu HH, Yan JX, Liang WH. Challenges and development prospects of ultra-long and ultra-deep mountain tunnels. Engineering 2019;5(3):384–92.
[3] Xu ZH, Liu FM, Lin P, Shao RQ, Shi XS. Nondestructive, *in-situ*, fast identification of adverse geology in tunnels based on anomalies analysis of element content. Tunn Undergr Space Technol 2021;118:104146.
[4] Zhang GH, Chen W, Jiao YY, Wang H, Wang CT. A failure probability evaluation method for collapse of drill-and-blast tunnels based on multistate fuzzy Bayesian network. Eng Geol 2020;276:105752.
[5] Huang F, Wu CZ, Ni PP, Wan GQ, Zheng AC, Jang BA, et al. Experimental analysis of progressive failure behavior of rock tunnel with a fault zone using non-contact DIC technique. Int J Rock Mech Min Sci 2020;132:104355.
[6] Liu JQ, Yuen KV, Chen WZ, Zhou XS, Wang W. Grouting for water and mud inrush control in weathered granite tunnel: a case study. Eng Geol 2020;279:105896.
[7] Chen YF, Liao Z, Zhou JQ, Hu R, Yang Z, Zhao XJ, et al. Non-Darcian flow effect on discharge into a tunnel in karst aquifers. Int J Rock Mech Min Sci 2020;130:104319.
[8] Gong QM, Yin LJ, Ma HS, Zhao J. TBM tunnelling under adverse geological conditions: an overview. Tunn Undergr Space Technol 2016;57:4–17.
[9] Lin P, Xiong Y, Xu ZH, Wang WY, Shao RQ. Risk assessment of TBM jamming based on Bayesian networks. Bull Eng Geol Environ 2022;81(1):47.
[10] Lin P, Yu TF, Xu ZH, Shao RQ, Wang WY. Geochemical, mineralogical, and microstructural characteristics of fault rocks and their impact on TBM jamming: a case study. Bull Eng Geol Environ 2022;81:64.
[11] Xu ZH, Wang WY, Lin P, Nie LC, Wu J, Li ZM. Hard-rock TBM jamming subject to adverse geological conditions: influencing factor, hazard mode and a case study of Gaoligongshan Tunnel. Tunn Undergr Space Technol 2021;108:103683.
[12] Lu CP, Liu B, Liu B, Liu Y, Wang HY, Zhang H. Anatomy of mining-induced fault slip and a triggered rockburst. Bull Eng Geol Environ 2019;78(7):5147–60.
[13] Sun YT, Li GC, Zhang JF, Huang JD. Rockburst intensity evaluation by a novel systematic and evolved approach: machine learning booster and application. Bull Eng Geol Environ 2021;80(11):8385–95.
[14] Li HJ, Li JH, Li L, Xu H, Wei JJ. Prevention of water and sand inrush during mining of extremely thick coal seams under unconsolidated Cenozoic alluvium. Bull Eng Geol Environ 2020;79(6):3271–83.
[15] Song WC, Liang ZZ. Theoretical and numerical investigations on mining-induced fault activation and groundwater outburst of coal seam floor. Bull Eng Geol Environ 2021;80(7):5757–68.
[16] Chen L, Shen BT, Dlamini B. Effect of faulting on coal burst—a numerical modelling study. Int J Min Sci Technol 2018;28(5):739–43.
[17] Vardar O, Zhang CG, Canbulat I, Hebblewhite B. A semi-quantitative coal burst risk classification system. Int J Min Sci Technol 2018;28(5):721–7.
[18] Li SC, Nie LC, Liu B. The practice of forward prospecting of adverse geology applied to hard rock TBM tunnel construction: the case of the Songhua River water conveyance project in the middle of Jilin Province. Engineering 2018;4(1):131–7.
[19] Lin P, Li SC, Xu ZH, Wang J, Huang X. Water inflow prediction during heavy rain while tunneling through karst fissured zones. Int J Geomech 2019;19(8):04019093.
[20] Xu ZH, Ma W, Lin P, Shi H, Pan DD, Liu TH. Deep learning of rock images for intelligent lithology identification. Comput Geosci 2021;154:104799.
[21] Xu ZH, Shi H, Lin P, Liu TH. Integrated lithology identification based on images and elemental data from rocks. J Petrol Sci Eng 2021;205:108853.
[22] He TX, Lu LZ, Li SX, Lan YQ. Metamorphic petrology. Beijing: Geology Press; 1980. Chinese.
[23] Solum J, Van der Pluijm B, Peacor D, Warr L. Influence of phyllosilicate mineral assemblages, fabrics, and fluids on the behavior of the Punchbowl fault, southern California. J Geophys Res 2003;108(B5):2233.
[24] Isaacs A, Evans J, Song SR, Kolesar P. Structural, mineralogical, and geochemical characterization of the Chelungpu thrust fault. Taiwan Terr Atmos Ocean Sci 2007;18(2):183–221.
[25] Duan QB, Yang XS, Ma SL, Chen JY, Chen JY. Fluid–rock interactions in seismic faults: implications from the structures and mineralogical and geochemical compositions of drilling cores from the rupture of the 2008 Wenchuan earthquake. China Tectonophysics 2016;666:260–80.
[26] Kanitpanyacharoen W, Chornkrathok S, Morley C, Wenk HR. Microstructural evolution and deformation mechanisms of Khao Kho Fault. Thailand J Struct Geol 2020;136:104055.
[27] Lin AM, Yamashita K. Spatial variations in damage zone width along strike-slip faults: an example from active faults in southwest Japan. J Struct Geol 2013;57:1–15.
[28] Wintsch R, Christoffersen R, Kronenberg AK. Fluid-rock reaction weakening of fault zones. J Geophys Res 1995;100(B7):13021–32.
[29] Haines S, Van der Pluijm B. Patterns of mineral transformations in clay gouge, with examples from low-angle normal fault rocks in the western USA. J Struct Geol 2012;43:2–32.
[30] Zhang GH, Jiao YY, Ma CX, Wang H, Chen LB, Tang ZC. Alteration characteristics of granite contact zone and treatment measures for inrush hazards during tunnel construction—a case study. Eng Geol 2018;235:64–80.
[31] Xu ZH, Yu TF, Lin P, Wang WY, Shao RQ. Integrated geochemical, mineralogical, and microstructural identification of faults in tunnels and its application to TBM jamming analysis. Tunn Undergr Space Technol 2022;128:104650.
[32] Zhang GH, Wang CT, Jiao YY, Wang H, Chen LB. Deposits sources of inrush hazards for the Liangshan Tunnel passing through deeply buried granite. Tunn Undergr Space Technol 2019;92:103058.
[33] Li SC, Xu ZH, Huang X, Lin P, Zhao XC, Zhang QS, et al. Classification, geological identification, hazard mode and typical case studies of hazard-causing structures for water and mud inrush in tunnels. J Rock Mech Eng 2018;37(5):1041–69. Chinese.
[34] Bounessah M, Atkin BP. An application of exploratory data analysis (EDA) as a robust non-parametric technique for geochemical mapping in a semi-arid climate. Appl Geochem 2003;18(8):1185–95.
[35] Lancianese V, Dinelli E. Different spatial methods in regional geochemical mapping at high density sampling: an application on stream sediment of Romagna Apennines. Northern Italy J Geochem Explor 2015;154:143–55.
[36] Zhou SG, Zhou KF, Cui Y, Wang JL, Ding JL. Exploratory data analysis and singularity mapping in geochemical anomaly identification in Karamay, Xinjiang. China J Geochem Explor 2015;154:171–9.
[37] Sarkar G, Banerjee S, Maity S, Srivastava HB. Fluid assisted rejuvenation of precursor brittle fractures as the habitats of ductile shear zones: an example from the ~2.6 Ga Bundelkhand Granitoid of north-central India. J Struct Geol 2020;141:104198.
[38] Goddard JM, Evans J. Chemical changes and fluid-rock interaction in faults of crystalline thrust sheets, northwestern Wyoming, USA. J Struct Geol 1995;17(4):533–47.
[39] Zhao PD, Chen YQ. Digital geology and quantitative mineral exploration. Earth Sci Front 2021;28(3):1–5. Chinese.
[40] Zuo RG. Data science-based theory and method of quantitative prediction of mineral resources. Earth Sci Front 2021;28:49–55. Chinese.
[41] Chapkanski S, Jacq K, Brocard G, Vittori C, Debret M, De Giorgi AU, et al. Calibration of short-wave infrared (SWIR) hyperspectral imaging using diffuse reflectance Infrared Fourier transform. Sediment Geol 2022;428:106062.
[42] Chen Q, Zhao ZF, Zhou JX, Zhu RF, Xia JS, Sun T, et al. Aster and Gf-5 satellite data for mapping hydrothermal alteration minerals in the Longtoushan Pb–Zn deposit, SW China. Remote Sens 2022;14(5):1253.
[43] De La Rosa R, Khodadadzadeh M, Tusa L, Kirsch M, Gisbert G, Tornos F, et al. Mineral quantification at deposit scale using drill-core hyperspectral data: a case study in the Iberian Pyrite Belt. Ore Geol Rev 2021;139:104514.
[44] He J, Barton I. Hyperspectral remote sensing for detecting geotechnical problems at Ray mine. Eng Geol 2021;292:106261.